

C-reactive Protein Detection Using an Ion-sensitive Field-effect Transistor (ISFET)-based Aptasensor with a Chemically Modified Gate Surface for Improved Sensitivity

Siti Masturah binti Fakhruddin,¹ Kumi Y. Inoue,^{2*}
Masayoshi Esashi,³ and Hitoshi Shiku⁴

¹Graduate School of Environmental Studies, Tohoku University, Sendai 980-8579, Japan

²Center for Basic Education, Faculty of Engineering, University of Yamanashi, Kofu 400-8511, Japan

³Micro System Integration Center (μSIC), Tohoku University, Sendai 980-0845, Japan

⁴Graduate School of Engineering, Tohoku University, Sendai 980-8579, Japan

(Received June 30, 2023; accepted October 12, 2023)

Keywords: aptamer, ion-sensitive field-effect transistor (ISFET), C-reactive protein, silane coupling, pH sensitivity

C-reactive protein (CRP) is an inflammation biomarker that requires simple and real-time monitoring for accurate diagnosis. Conventional CRP tests are complicated, expensive, and time-consuming. Field-effect transistor (FET)-based affinity sensors are seen as the ideal solution but it is difficult to obtain FET with sensitive gate structures. In this work, we propose a simple method of chemically modifying the gate surface of a commercial ion-sensitive FET (ISFET) with (3-glycidyoxypropyl)trimethoxysilane (GPTMS) to lower the background noise signal and then immobilize aptamers that provide significant surface potential change when they bind to CRP. The FET aptasensor was able to measure 0.002–20 μg/mL CRP in 1 × phosphate-buffered saline (PBS) with a higher sensitivity than the nonmodified ISFET sensors with their original pH sensitivity and was on par with other FET sensors without needing expensive nanomaterial or complicated nanofabrication.

1. Introduction

C-reactive protein (CRP) is a pentameric plasma protein produced by the liver and can be found in blood and certain other biofluids. It is an acute-phase protein and nonspecific biomarker that can indicate the levels of inflammation and tissue damage in the body. Monitoring CRP levels can be useful for assessing cardiovascular risks or even COVID-19 infection severity (1 ng/mL for very mild cases to more than 100 ng/mL).⁽¹⁾ Plasma levels of CRP in humans can rise rapidly more than 1000-fold after an acute-phase stimulus, and the synthesis rate peaks around 48 h.^(2,3) Furthermore, the plasma half-life of CRP is about 19 h, making it difficult to monitor accurately in patients. This makes it necessary to have a sensor that can measure the real-time and long-term CRP levels of patients to obtain accurate diagnostic results. The real-

*Corresponding author: e-mail: inokumi@yamanashi.ac.jp
<https://doi.org/10.18494/SAM4570>

time monitoring of CRP levels in patients is also vital for medical events such as cytokine storms that occur in COVID-19 patients.^(4–6) CRP level has even been found to be predictive of survival rate among high-risk COVID-19 patients.⁽⁷⁾

Conventional methods of measuring CRP levels in blood serum include enzyme-linked immunoassay (ELISA), high-sensitivity assay, and cardiac assay, with limits of detection varying from 0.03 to 0.2 $\mu\text{g/mL}$ and detection ranges up to 10 $\mu\text{g/mL}$.⁽⁸⁾ These methods require complicated labeling materials, multistep processes, expensive equipment, and experienced personnel. To overcome these limitations, there have been multiple different approaches in developing CRP sensors such as fluorescence,⁽⁹⁾ surface plasmon resonance (SPR),^(10,11) electrochemical methods^(12,13) or even acoustic profiling/quartz crystal microbalance.⁽¹⁴⁾ However, these methods still have disadvantages such as requiring fluorescent labels, complicated fabrication process, and expensive equipment with skilled personnel for operation. They are also incapable of real-time measurements. Thus, field-effect transistor (FET)-based sensors that offer rapid and label-free direct electrical detection, inexpensive mass production with easy miniaturization, and relative ease of use are gaining interest to realize the need for a CRP sensor capable of point-of-care diagnostics.

Since the invention of the metal-oxide-semiconductor FET (MOSFET) in 1959, a myriad of FET-based sensors with different structures, sensing materials, and their target analytes have been developed. The ion-sensitive FET (ISFET) itself was introduced by Bergveld in 1970⁽¹⁵⁾ and derived from the MOSFET structure. In practice, ISFET sensors are often operated in a constant charge or constant drain-current mode, i.e., by setting the drain current at a fixed value using a feedback circuit, the resulting sensor output signal from the biochemical reaction is then proportional to the voltage shift recorded.⁽¹⁶⁾ However, FET sensors have inherent limitations such as the Debye screening length (counter-ion screening effect), which occurs during measurements in an aqueous medium, and that the sensitive detection of biomolecules with low or neutral charges is difficult without some form of interaction that can significantly affect the surface potential of the FET sensor.

Some of the earliest attempts of FET-based CRP sensors were by Sohn *et al.* in 2007,⁽¹⁷⁾ Sohn and Kim in 2008,⁽¹⁸⁾ and Lyu *et al.* in 2009.⁽¹⁹⁾ Their techniques mostly used the extended-gate FET configuration where the gate electrode is connected to the sensing layer that is physically external to the FET itself. CRP detection occurs when negatively charged CRP binds to the CRP antibodies immobilized on the gate surface, and this induces a change in drain-source current. To improve the sensor's limit of detection and detection range, especially in physiological fluids (high ionic strength), sensing methods have been proposed over the years with varying levels of success. Examples are silicon nanowire FET CRP sensors developed by Lee,⁽²⁰⁾ Lee *et al.*,⁽²¹⁾ and Kwon *et al.*,⁽²²⁾ the nanogap-embedded FET proposed by Ahn *et al.*⁽²³⁾ and Kim *et al.*,⁽²⁴⁾ a hybrid MOSFET with a bipolar junction transistor,^(25,26) a carbon nanotube FET,⁽²⁷⁾ and an AlGaIn/GaN high-electron-mobility transistor (HEMT),^(28,29) which was also combined with a microfluidic platform, an electrolyte-gated organic FET sensor,⁽³⁰⁾ or a different oxide material for the gate electrode.⁽³¹⁾ These sensors were mostly focused on nanotechnology or gate oxide material to improve their capabilities. This required complicated fabrication steps or expensive nanomaterials that can hinder the mass production of the sensors.

On the other hand, ISFETs are readily and inexpensively available on the market. ISFETs for pH sensing have a pH sensitivity of about 56–58 mV/pH, which originated from the protonation and deprotonation of the –OH groups of their gate material, such as Ta₂O₅.^(32,33) This means that the sensor is easily affected by pH. Therefore, by eliminating the –OH groups on the gate surface of a commercial ISFET and adding a CRP biorecognition layer to the gate surface, a CRP sensor can be mass-produced by taking advantage of the commercial ISFET sensor. Furthermore, most of the FET-based CRP sensors were immunosensors and used anti-CRP antibodies as the biorecognition layer. Antibodies (about 10 nm) are larger than the Debye length of physiological fluids (about 0.7 nm), which requires the sensors to use diluted solutions or nanotechnology as mentioned previously. Aptamer-based FET sensors for CRP detection only emerged in 2015.^(34–36) Aptamers are synthetic oligonucleotides that are smaller than antibodies; therefore, their interactions with the target analyte are more likely to be within the Debye screening length. Aptamers' backbones are made up of negatively charged phosphate groups; therefore, biomolecules binding to the aptamers will enable signal transduction and amplification even for biomolecules with low or neutral charges.

In this work, we propose a simple method of chemically modifying the gate surface of a commercial ISFET with silane coupling agents to eliminate the –OH groups on the gate surface to reduce pH sensitivity, which is indirectly the background signals. CRP-binding aptamers are used as the biorecognition layer. To the best of our knowledge, this work is the first to propose the method of decreasing the pH sensitivity of the gate material to increase the sensitivity of the FET CRP sensor.

2. Data, Materials, and Methods

2.1 Reagents and solutions

Human CRP full length protein (ABI67710) was purchased from Abcam. The CRP-binding aptamer with amine-terminated end 5'-GGCAGGAAGACAAACACGATGGGGGGGTATGATTTGATGTGGTTGTTGCATGATCGTGGTCTGTGGTGCTGT-3'^(37,38) with a binding affinity of $K_d = 3.51$ nM was manufactured by Eurofin Genomics. (3-Glycidyloxypropyl)trimethoxysilane (GPTMS) was purchased from Sigma-Aldrich and (3-aminopropyl)trimethoxysilane (APTMS) from Tokyo Chemical Industry (TCI). Phosphate-buffered saline [PBS(-)] was purchased from Nacalai Tesque. Phosphate pH standard equimolar solution, 25% glutaraldehyde, ethanolamine, acetone, isopropanol, and ethanol were purchased from Fujifilm Wako Pure Chemical. All aqueous solutions in this study were prepared using Milli-Q water (Millipore Corp.).

2.2 Device fabrication and biofunctionalization

The ISFET sensors were purchased from ISFETCOM Co., Ltd., Japan (Fig. 1). The ISFET sensor was first ultrasonicated up to 10 s in pure water, acetone, and isopropanol, in this sequence. It then undergoes plasma ashing at 70 W for 60 s. The cleaned ISFET sensor was

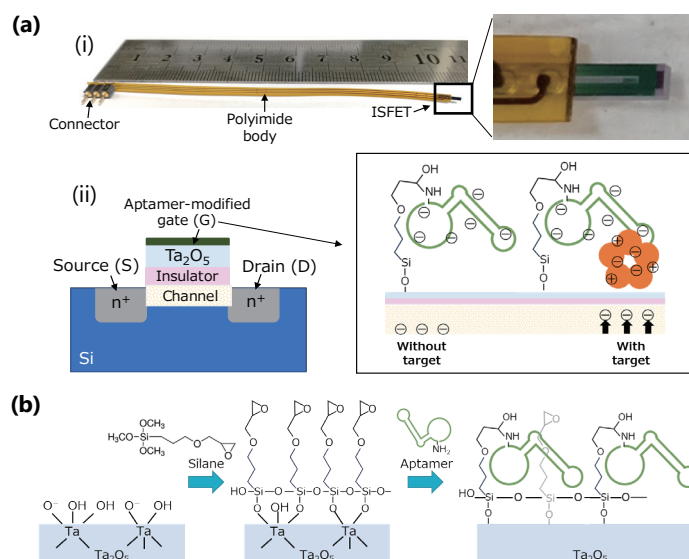


Fig. 1. (Color online) (a, i) ISFET aptasensor with a closeup of the ISFET sensing chip. (a, ii) Simplified schematic of the ISFET aptasensor and detection mechanism. (b) Biofunctionalization steps of the ISFET sensor.

silanized by gas-phase silanization with either (i) 400 μL of GPTMS for 2 h at 80 $^{\circ}\text{C}$ in vacuum or (ii) 400 μL of APTMS overnight at room temperature in vacuum. A physically adsorbed FET aptasensor was fabricated by (iii) incubating the cleaned ISFET with the CRP-binding aptamer (2 μM) overnight at room temperature. Silanized ISFET sensors were rinsed with anhydrous ethanol to remove unreacted silane from the ISFET surface before the CRP-binding aptamer (2 μM) was then reacted with the silanized surface overnight at room temperature. Afterwards, PBS was used to rinse the ISFET before immersing in 50 mM ethanolamine as blocking buffer overnight at room temperature. Further rinse using PBS was performed before the ISFET was used for CRP detection.

2.3 ISFET pH sensitivity evaluation and CRP quantitative measurement

The ISFET is connected to the customized measuring apparatus and a commercial Ag/AgCl (sat. KCl) reference electrode (BAS Inc., USA). It is first calibrated to 0.0 V in pH 6.86 phosphate pH standard equimolar solution at room temperature before adding 0.1 M NaOH or 0.1 M HCl to the pH 6.86 standard buffer solution to change the pH, and thus the voltage, accordingly. The pH of the solution is recorded using a pH meter (Mettler Toledo, Belgium). Aptamer-modified ISFETs are calibrated to 0.0 V using PBS solution to prevent harming the aptamer layer. 0.1 M NaOH or 0.1 M HCl is then added to the PBS solution to change its pH.

CRP detection is carried out almost similarly. First, the ISFETs are calibrated to 0 V in PBS solution (pH 7.4), i.e., 0 $\mu\text{g/mL}$ solution, before being incubated for 30 min in 0.002, 0.02, 0.2, 2, 5, 10, and 20 $\mu\text{g/mL}$ CRP solutions (diluted in PBS), in that order. The ISFETs are rinsed thoroughly in PBS in between measurements. These steps are then repeated using $0.1 \times$ PBS and $0.01 \times$ PBS solutions to investigate the Debye screening effect.

3. Results and Discussion

3.1 Silanization of ISFET surface of Ta₂O₅ and immobilization of aptamer

We opted to use silanization, a method that will simultaneously lessen the density of –OH groups and enable aptamer immobilization. The conventional silane often used for the FET surface is aminosilane (APTMS or APTES), which has a positively charged amine group at one end to immobilize proteins using a crosslinking agent. This is detrimental to our strategy of reducing the pH sensitivity of the FET sensor; hence, we chose to use epoxysilane (GPTMS) that can also facilitate aptamer immobilization without the need for a crosslinking reagent. We also conducted silanization using APTMS as a control. AFM and XPS measurements were used to evaluate untreated and silane-treated surfaces, and the results are shown in Fig. 2. Since the FET sensors were very small for the measurements, we used samples fabricated using Ta₂O₅ sputtered on Si wafers instead. The peak changes in XPS data (for Si 2p and 2s) between untreated Ta₂O₅ and GPTMS-treated Ta₂O₅ clearly indicate the formation of a silane layer on the Ta₂O₅ surface. Further aptamer immobilization shows the appearance of a N peak, which can be attributed to the amine group of the aptamer (Table 1).

A more detailed discussion can be made using the composition ratio summarized from the overall XPS data (note that the composition ratio is only for rough comparisons and not accurate

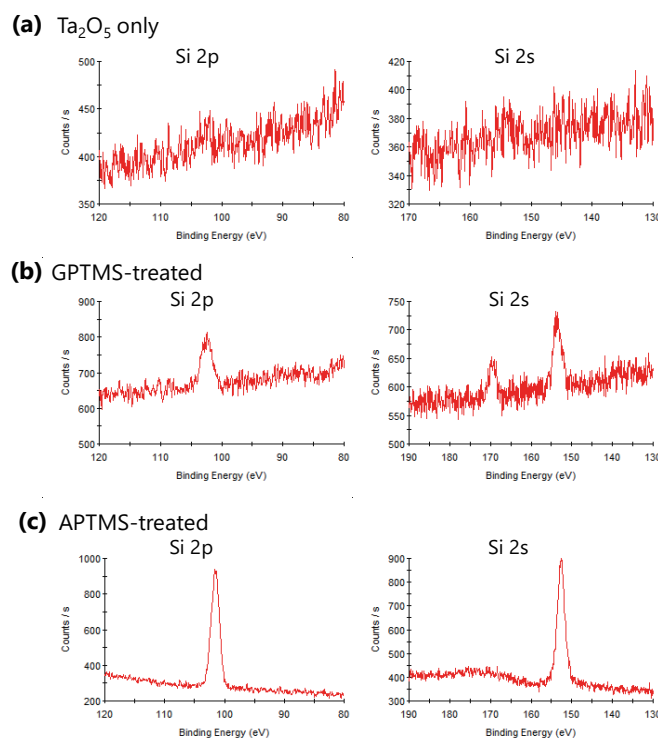


Fig. 2. (Color online) Surface modification evaluation by XPS, Si2p, and 2s scans. (a) Untreated Ta₂O₅ surface, (b) GPTMS-treated Ta₂O₅ surface, and (c) APTMS-treated Ta₂O₅ surface.

Table 1
Composition ratio summary from XPS data.

	Ta (4f)	Si (2p, 2s)	O (1s)	C (1s)	P (2p)	N (1s)
Untreated	0.27	0.01	0.64	0.08	—	—
APTMS	0.01	0.16	0.22	0.44	0.00	0.10
GPTMS	0.13	0.03	0.39	0.10	0.00	0.33
Apt	0.14	0.01	0.39	0.04	0.02	0.36
APTMS-GA-Apt	0.00	0.08	0.19	0.60	0.01	0.08
GPTMS-Apt	0.14	0.03	0.38	0.07	0.00	0.37

descriptions of the surfaces measured). Silanization using either APTMS or GPTMS results in a decrease in Ta composition rate and an increase in Si, O, or C composition ratio, which indicate that Ta-OH is now replaced by Ta-O-Si-CH₃ instead. Hence, it can be considered that both silanes can reduce the density of -OH groups on the Ta₂O₅ surface. However, APTMS showed a more marked Ta decrease and Si increase in composition ratio compared with GPTMS. We consider that this is because the reaction time for APTMS is much longer than that for GPTMS (overnight compared to 2), which led to an increase in the vertical polymerization of APTMS leading to the formation of 3D “islands” compared with mostly horizontal polymerization for GPTMS.^(39,40) APTMS also has a short carbon chain, which meant that it is more prone to 3D polymerization as reaction time is increased. Therefore, GPTMS is more successful in forming a thin silane layer than APTMS, which is also effective in lowering pH sensitivity as explained in the next section. P and N data for both APTMS and GTPMS are also shown. Since they are not modified with aptamers, P is undetectable for both APTMS- and GPTMS-treated surfaces. A slight increase in N composition ratio is seen in the APTMS-treated surface, which originated from the amine groups of APTMS itself. However, the unexpected increase in N for the GPTMS-treated surface can only be attributed to possible cross-contamination from the vacuum container due to prior aminosilane treatment, since GPTMS nor the chemicals used during the epoxysilane treatment have any N group. (This vacuum container was not used for the next GPTMS-treated and aptamer-immobilized Ta₂O₅ surface; hence, the results can be properly attributed to the modification treatment.)

Aptamer immobilization is then confirmed by scanning for P and N, which are the phosphate groups in the aptamer’s backbone and the amine group at one end of the aptamer (Table 1). For the APTMS-treated and aptamer-immobilized Ta₂O₅ surface, P and N were both confirmed; however, interestingly, the Ta composition ratio was effectively zero. We attributed this to the formation of the said “islands” and the aptamer immobilization (physical adsorption of aptamer on the untreated Ta₂O₅ surface also reduced the Ta and O composition ratios) having physically covered the Ta₂O₅ surface such that Ta was undetectable (for that specific point of measurement). Note that the N composition ratio was lower than that of the physically adsorbed aptamer on the untreated Ta₂O₅ surface. Considering that the APTMS itself also has amine groups, we concluded that the formation of 3D islands reduced the number of viable sites for aptamer immobilization; hence, a lower number of aptamers were immobilized compared with physically adsorbed and GPTMS-treated aptamer modifications.

In contrast, while N was detected (at about the same level as for physically adsorbed aptamers on the untreated Ta₂O₅ surface) for the GPTMS-treated and aptamer-immobilized Ta₂O₅ surface, P was effectively undetectable (too low to be detected but not exactly zero). However, P can be difficult to detect since the aptamer backbone where the phosphate groups are located can be in a rolled-up or loose configuration, as indicated by the low ratios for both physically adsorbed and APTMS-treated aptamer modifications. Hence, the GPTMS-treated aptamer modification can be considered to have a structure different from those of the other two methods.

3.2 Reducing pH sensitivity for lower background signals

We also investigated how the silane surface treatment affected the pH sensitivity by measuring the pH dependence on the surface potential of the ISFET, i.e., its output voltage. As shown in Fig. 3, GPTMS reduced the pH sensitivity better than APTMS. From the untreated FET sensor with a sensitivity of about 56.2 mV/pH, it dropped to about 54.4 mV/pH after the GPTMS treatment. This can be attributed to the –OH groups becoming reduced by the silanization reaction, combined with the slightly negative charge of the epoxy group that did not particularly affect the pH sensitivity of the FET sensor. The subsequent treatment with the NH₂-terminated CRP-binding aptamer and blocking buffer ethanolamine caused further increase and decrease in pH sensitivity, which can be considered as the effects of the following:

- i. the amine-terminated aptamer bonding with the epoxy group to create neutral charges and
- ii. the ethanolamine that has its amine side bonded with unreacted epoxy groups but has a free –OH side itself.

Overall, the GPTMS treatment helped reduce the pH sensitivity of the FET sensor. Conversely, even with –OH groups reduced by silanization, the APTMS treatment had slightly increased the pH sensitivity instead, which is due to the positive charges of the amine group. Further functionalization steps did not significantly change the pH sensitivity of the pH sensor either.

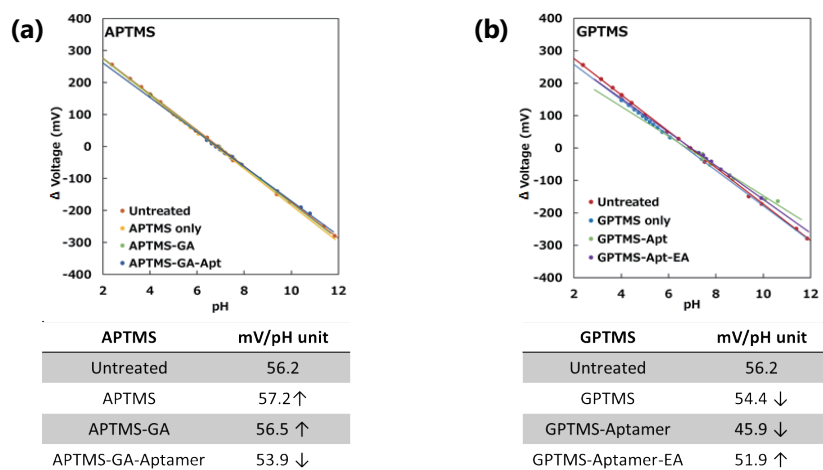


Fig. 3. (Color online) Gate surface potential shift of the FET by pH change from pH 7.0 for pH sensitivity evaluation of the (a) APTMS-treated and (b) GPTMS-treated FETs.

3.3 CRP detection in $1 \times$ PBS

Modified and nonmodified FET sensors or aptasensors (aptamer-modified sensors) were then used to detect 0, 0.002, 0.02, 0.2, 2, 5, 10, and 20 $\mu\text{g/mL}$ CRP, and the results are shown in Fig. 4. A physiological ionic strength solution was used to provide practical results in terms of feasibility as a point of care (POC) biosensor. The epoxysilane-treated FET aptasensor (GPTMS-apt) successfully detected down to 0.002 $\mu\text{g/mL}$ CRP with a more distinguishable and higher signal strength between CRP concentrations than the other FET sensors. The aminosilane-treated FET aptasensor (APTMS-apt) was only able to clearly detect CRP from 2 $\mu\text{g/mL}$ onwards. The nonsilanized physically adsorbed aptasensor (bFET-apt) and untreated blank FET sensor (blank-FET) were only able to start detecting CRP from 5 $\mu\text{g/mL}$ onwards. Since the CRP level between 1 and 3 $\mu\text{g/mL}$ is considered as medium risk and more than 3 $\mu\text{g/mL}$ is already high risk, APTMS-apt, bFET-apt, and blank-FET were not practical for POC biosensor use. Instead, GPTMS-apt that was able to detect CRP levels ranging from 0.002 to 20 $\mu\text{g/mL}$ in physiological ionic strength solution showed its feasibility as a POC CRP biosensor. To reiterate, this GPTMS-treated FET aptasensor did not need expensive nanomaterial modifications or a complicated nanostructure fabrication to achieve its current sensitivity and measurement range, compared with other FET sensors for CRP detection (Table 2). Furthermore, the GPTMS-treated FET aptasensor was capable of measuring the current CRP concentration range in $1 \times$ PBS, a high-ionic-strength solution, compared with other FET biosensors for CRP, which resorted to measuring under dry conditions^(24,27) to circumvent the Debye screening effect.

3.4 CRP detection in solutions with different Debye screening lengths

The performance of the GPTMS-treated FET aptasensor was evaluated in PBS with different ionic strengths and the results are shown in Fig. 5. The FET aptasensor shows increased signal strength in solutions with low ionic concentrations. This is because when the solution has fewer buffer ions, the counter-ion screening effect becomes weaker and the effective measuring

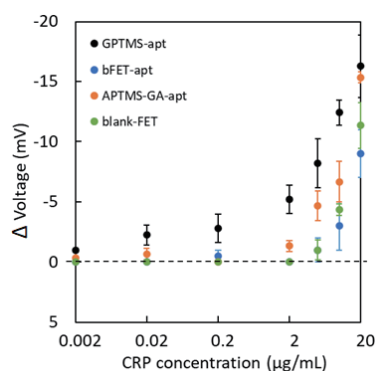


Fig. 4. (Color online) Gate voltage change during CRP detection after calibration to 0 V in 0 $\mu\text{g/mL}$ solution for comparison of CRP detection sensitivity between ISFETs in $1 \times$ PBS. Error bars represent the standard deviations ($n = 3$).

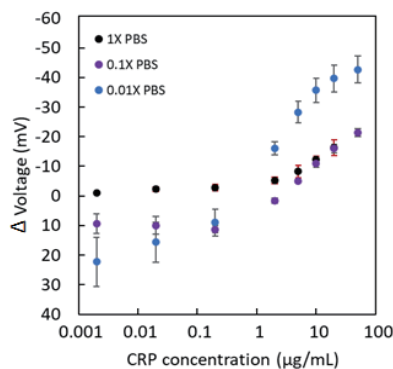
Table 2

This work in comparison with other FET and non-FET biosensors for CRP.

Sensor type	Ligand	Experimental conditions	Detection time ^{*1}	Detection range	Limit of detection ^{*2}
This work	aptamer	1 × PBS	35 min	0.002–20 µg/mL	0.002 µg/mL
Extended gate FET ⁽¹⁷⁾	antibody	unidentified	—	3–10 µg/mL	—
Nanogap conventional SiO ₂ FET ⁽²⁴⁾	antibody	dry	20 min	0–100 ng/mL	0.1 ng/mL
AlGa _N /Ga _N HEMT with null-balancing circuit ⁽²⁸⁾	antibody	1 × PBS	3 h	10–1000 ng/mL	10 ng/mL
Cysteine-tagged protein G modified Au/NiCr gated FET ⁽¹⁸⁾	antibody	unidentified	—	3–20 µg/mL	—
SiO ₂ -CeO ₂ ISFET ⁽³¹⁾ (biotin/streptavidin/Ab)	antibody	1 × PBS	30 min	0.1–2.5 µg/mL	0.1 µg/mL
Carbon nanofiber immunoassay + EIS ⁽⁴¹⁾	antibody	1 × PBS	80 min	0.05–5 µg/mL	0.011 µg/mL
Magnetic NP + micro fluxgate sensor ⁽⁴²⁾ (magnetic field)	antibody	1 × PBS	30 min	0.002–10 µg/mL	0.002 µg/mL
SWCNT SiO ₂ Ti/Au FET ⁽²⁷⁾	antibody	dry	20 min	0.001–100 µg/mL	0.001 µg/mL
Polymer-modified organic FET ⁽³⁰⁾ (physical adsorption)	antibody	1 × PBS	15 min	0.4 ng/mL–0.2 mg/mL	0.22 ng/mL

*1: Estimated as a total reaction time including incubation time for CRP and ligand binding, washing time, and measurement time from the experimental procedure in each paper.

*2: Value as written in each reference was adopted. Generally, the limit of detection is the lowest analyte concentration where the signal exceeds "BG + 3σ", derived from background (BG: an averaged signal at zero analyte) and standard deviation at zero analyte (σ). In this work, the limit of detection is defined as the lowest concentration where the entire error bar is within the positive region.



PBS	Ionic strength (mM)	Debye length (nm)	pH
1X	162.7	0.76	7.4
0.1X	16.27	2.41	7.4
0.01X	1.627	7.61	7.4

Approximate composition of 1x PBS buffer: 138 mM NaCl, 2.7 mM KCl, 1.9 mM NaH₂PO₄, 8.1 mM Na₂HPO₄

Fig. 5. (Color online) Gate voltage change during CRP detection in PBS with different ionic strengths (1×, 0.1×, 0.01×) using GPTMS-treated FET aptasensors. Error bars represent the standard deviations ($n = 3$). The FET aptasensors were first calibrated to 0 V in 0 µg/mL solution.

distance becomes shorter. Interestingly, although the FET aptasensors were calibrated to 0 V in 0 µg/mL CRP (either 1×, 0.1×, or 0.01 × PBS), low concentrations of CRP in 0.1× and 0.01 × PBS gave a positive potential output that grows increasingly negative with increasing CRP concentration, instead of starting with a negative potential output. This phenomenon can be attributed to the fact that the same concentration of CRP is present with increasingly fewer

buffer ions in each ionic strength solution, which meant increased effective measuring distance. Hence, the slightly negative charges of the CRP itself also affected the gate surface potential. This and combined with the CRP concentration being too low to cause significant conformational changes in the aptamer thus gave the positive potential output for low CRP concentrations. Therefore, as the CRP concentration increased and the aptamer conformational changes significantly contributed to gate surface potential changes, the potential output becomes increasingly negative. Furthermore, the output signals for $0.1 \times$ PBS did not significantly increase compared with the output signals for $1 \times$ PBS. This may have been due to fewer buffer ions affecting the binding of CRP to the aptamer. Since CRP is slightly negatively charged, without some shielding effect from the buffer ions, electrostatic repulsion may have occurred between the negatively charged phosphate backbone of the aptamer and the CRP itself, affecting the FET aptasensor's detection sensitivity. In other words, aptamer binding is largely mediated by electrostatic forces.^(42–44) Hence, the limits of detection for $0.1 \times$ PBS and $0.01 \times$ PBS differ from that of $1 \times$ PBS ($5 \mu\text{g/mL}$ for $0.1 \times$ PBS and $2 \mu\text{g/mL}$ for $0.01 \times$ PBS).

4. Conclusions

In this work, a novel concept for increasing the signal sensitivity of a FET aptasensor using easy and low-cost modification methods is proposed. The FET aptasensor treated with GPTMS by gas-phase silanization and then aptamer-functionalized was able to measure $0\text{--}20 \mu\text{g/mL}$ CRP in $1 \times$ PBS solution (physiological ionic strength) with a higher signal sensitivity than those of other (modified or nonmodified) FET sensors. Furthermore, the FET aptasensor did not require expensive nanomaterial modifications or a complicated nanostructure fabrication to achieve its current sensitivity and measurement range, compared with other FET sensors for CRP detection. However, the confirmation of specificity and investigation using clinical samples such as spike and recovery tests using blood and serum remain. We will proceed with further studies including these evaluations to realize a low-cost and practical CRP sensor for accurate disease monitoring.

Acknowledgments

This research was supported by JST COI (no. JPMJCE1303) from the Japan Science and Technology Agency (JST). This research was also supported partly by AMED Grant Number JP21zf0127001 from the Japan Agency for Medical Research and Development (AMED). It was also partially supported by a Grant-in-Aid for Scientific Research (B) (no. 22H02105) and a Grant-in-Aid for Challenging Research (Exploratory) (no. 22K18941) from the Japan Society for the Promotion of Science (JSPS) and JST FOREST Program (no. JPMJFR213C) from JST. We would like to express our thanks to Professor Nagatomi Ryoichi and Professor Yoshida Shinya for their input on the need for CRP monitoring and on using FET biosensing. We are also grateful to the Nishizawa Memorial Centre for allowing the use of their sputtering machinery and to the Instrumental Analysis Group of Tohoku University for the XPS and AFM measurements and their invaluable insight.

References

- 1 M. Kermali, R. K. Khalsa, K. Pillai, Z. Ismail, and A. Harky: *Life Sci.* **254** (2020) 117788. <https://doi.org/10.1016/j.lfs.2020.117788>
- 2 M. B. Pepys and G. M. Hirschfield: *J. Clin. Invest.* **112** (2003) 299. <https://doi.org/10.1172/JCI200318921>
- 3 S. Black, I. Kushner, and D. Samols: *J. Biol. Chem.* **279** (2004) 48487. <https://doi.org/10.1074/jbc.R400025200>
- 4 L. Yan, H.-T. Zhang, J. Goncalves, Y. Xiao, M. Wang, Y. Guo, C. Sun, X. Tang, L. Jing, M. Zhang, X. Huang, Y. Xiao, H. Cao, Y. Chen, T. Ren, F. Wang, Y. Xiao, S. Huang, X. Tan, N. Huang, B. Jiao, C. Cheng, Y. Zhang, A. Luo, L. Mombaerts, J. Jin, Z. Cao, S. Li, H. Xu, and Y. Yuan: *Nat. Mach. Intell.* **2** (2020) 283. <https://doi.org/10.1038/s42256-020-0180-7>
- 5 R. Caricchio, M. Gallucci, C. Dass, X. Zhang, S. Gallucci, D. Fleece, M. Bromberg, and G. J. Criner: *Ann. Rheum. Dis.* **80** (2021) 88. <https://doi.org/10.1136/annrheumdis-2020-218323>
- 6 D. M. Del Valle, S. Kim-Schulze, H. H. Huang, N. D. Beckmann, S. Nirenberg, B. Wang, Y. Lavin, T. H. Swartz, D. Madduri, A. Stock, T. U. Marron, H. Xie, M. Patel, K. Tuballes, O. Van Oekelen, A. Rahman, P. Kovatch, J. A. Aberg, E. Schadt, S. Jagannath, M. Mazumdar, A. W. Charney, A. Firpo-Betancourt, D. R. Mendu, J. Jhang, D. Reich, K. Sigel, C. Cordon-Cardo, M. Feldmann, S. Parekh, M. Merad, and S. Gnjatic: *Nat. Med.* **26** (2020) 1636. <https://doi.org/10.1038/s41591-020-1051-9>
- 7 A. Villoteau, M. Asfar, M. Oteko, J. Loison, J. Gautier, and C. Annweiler: *PLoS One* **16** (2021) 1. <https://doi.org/10.1371/journal.pone.0256931>
- 8 FDA, Guid. Ind. FDA Staff 2005, 1–114.
- 9 K. M. Park, D. J. Chung, M. Choi, T. Kang, and J. Jeong: *Nano Converg.* **6** (2019) 35. <https://doi.org/10.1186/s40580-019-0207-0>
- 10 Y. H. Choi, H. Ko, G. Y. Lee, S. Y. Chang, Y. W. Chang, M. J. Kang, and J. C. Pyun: *Sens. Actuators, B* **207** (2015) 133. <https://doi.org/10.1016/j.snb.2014.10.012>
- 11 W. Wang, Z. Mai, Y. Chen, J. Wang, L. Li, Q. Su, X. Li, and X. Hong: *Sci. Rep.* **7** (2017) 16904. <https://doi.org/10.1038/s41598-017-17276-3>
- 12 S. Centi, L. B. Sanmartin, S. Tombelli, I. Palchetti, and M. Mascini: *Electroanalysis* **21** (2009) 1309. <https://doi.org/10.1002/elan.200804560>
- 13 M. Jarczewska, R. Ziółkowski, Ł. Górski, and E. Malinowska: *Electroanalysis* **30** (2018) 658. <https://doi.org/10.1002/elan.201700620>
- 14 J. D. McBride and M. A. Cooper: *J. Nanobiotechnology* **6** (2008) 2. <https://doi.org/10.1186/1477-3155-6-5>
- 15 P. Bergveld: *IEEE Trans. Biomed. Eng.* **BME-17** (1970) 70. <https://doi.org/10.1109/TBME.1970.4502688>
- 16 M. J. Schöning and A. Poghossian: *Analyst* **127** (2002) 1137. <https://doi.org/10.1039/b204444g>
- 17 Y.-S. Sohn, S. K. Lee, and S.-Y. Choi: *Sens. Lett.* **5** (2007) 421. <https://doi.org/10.1166/sl.2007.216>
- 18 Y.-S. Sohn and Y. T. Kim: *Electron. Lett.* **44** (2008) 955. <https://doi.org/10.1049/el:20080720>
- 19 H.-K. Lyu, Y.-S. Choi, J.-K. Shin, and J.-H. Kim: *Smart Biomed. Physiol. Sens. Technol.* VI, B. M. Cullum and D. M. Porterfield, Eds. (SPIE, 2009) p. 73130S.
- 20 M.-H. Lee: *Int. J. Nanomedicine* **3** (2008) 117. <https://doi.org/10.2147/IJN.S2437>
- 21 M.-H. Lee, D.-H. Lee, S.-W. Jung, K.-N. Lee, Y. S. Park, and W.-K. Seong: *Nanomedicine Nanotechnol. Biol. Med.* **6** (2010) 78. <https://doi.org/10.1016/j.nano.2009.04.004>
- 22 S. M. Kwon, G. B. Kang, Y. T. Kim, Y.-H. Kim, and B.-K. Ju: *J. Nanosci. Nanotechnol.* **11** (2011) 1511. <https://doi.org/10.1166/jnn.2011.3417>
- 23 J. H. Ahn, J. Y. Kim, M. Im, J. W. Han, and Y. K. Choi: in *14th Int. Conf. Miniaturized Systems for Chemistry and Life Sciences 2010, MicroTAS 2010* (2010) 1301.
- 24 C. H. Kim, J. H. Ahn, J. Y. Kim, J. M. Choi, K. C. Lim, T. Jung Park, N. Su Heo, H. Gu Lee, J. W. Kim, and Y. K. Choi: *Biosens. Bioelectron.* **41** (2013) 322. <https://doi.org/10.1016/j.bios.2012.08.047>
- 25 H. M. Jeong, J. B. Kwon, H. C. Kwon, J. S. Kim, B. Xu, D. H. Kwon, and S. W. Kang: *IEEE Trans. Electron Devices* **65** (2018) 243. <https://doi.org/10.1109/TED.2017.2777603>
- 26 H. Yuan, H. C. Kwon, S. H. Yeom, D. H. Kwon, and S. W. Kang: *Biosens. Bioelectron.* **28** (2011) 434. <https://doi.org/10.1016/j.bios.2011.07.062>
- 27 C. I. L. Justino, A. C. Freitas, J. P. Amaral, T. A. P. Rocha-Santos, S. Cardoso, and A. C. Duarte: *Talanta* **108** (2013) 165. <https://doi.org/10.1016/j.talanta.2013.03.007>
- 28 H. H. Lee, M. Bae, S. H. Jo, J. K. Shin, D. H. Son, C. H. Won, H. M. Jeong, J. H. Lee, and S. W. Kang: *Sensors (Switzerland)* **15** (2015) 18416. <https://doi.org/10.3390/s150818416>
- 29 H. H. Lee, M. Bae, S. H. Jo, J. K. Shin, D. H. Son, C. H. Won, and J. H. Lee: *Sens. Actuators, B* **234** (2016) 316. <https://doi.org/10.1016/j.snb.2016.04.117>
- 30 M. Magliulo, D. De Tullio, I. Vikholm-Lundin, W. M. Albers, T. Munter, K. Manoli, G. Palazzo, and L. Torsi: *Anal. Bioanal. Chem.* **408** (2016) 3943. <https://doi.org/10.1007/s00216-016-9502-3>

- 31 O. Kutova, M. Dusheiko, N. I. Klyui, and V. A. Skryshevsky: *Microelectron. Eng.* **215** (2019) 110993. <https://doi.org/10.1016/j.mee.2019.110993>
- 32 M. Yuqing, G. Jianguo, and C. Jianrong: *Biotechnol. Adv.* **21** (2003) 527. [https://doi.org/10.1016/S0734-9750\(03\)00103-4](https://doi.org/10.1016/S0734-9750(03)00103-4)
- 33 T. Matsuo and M. Esashi: *Sensors and Actuators* **1** (1981) 77. [https://doi.org/10.1016/0250-6874\(81\)80006-6](https://doi.org/10.1016/0250-6874(81)80006-6)
- 34 C.-H. Chu, I. Sarangadharan, A. Regmi, Y.-W. Chen, C.-P. Hsu, W.-H. Chang, G.-Y. Lee, J.-I. Chyi, C.-C. Chen, S.-C. Shiesh, G.-B. Lee, and Y.-L. Wang: *Sci. Rep.* **7** (2017) 5256. <https://doi.org/10.1038/s41598-017-05426-6>
- 35 A. Sinha, T.-Y. Tai, K.-H. Li, P. Gopinathan, Y.-D. Chung, I. Sarangadharan, H.-P. Ma, P.-C. Huang, S.-C. Shiesh, Y.-L. Wang, and G.-B. Lee: *Biosens. Bioelectron.* **129** (2019) 155. <https://doi.org/10.1016/j.bios.2019.01.001>
- 36 C.-H. Chu, W.-H. Chang, W.-J. Kao, C.-L. Lin, K.-W. Chang, Y.-L. Wang, and G.-B. Lee: *IEEE International Conference on Micro Electro Mechanical Systems (IEEE, 2015)* 581–584.
- 37 C. J. Huang, H. I. Lin, S. C. Shiesh, and G. Bin Lee: *Biosens. Bioelectron.* **25** (2010) 1761. <https://doi.org/10.1016/j.bios.2009.12.029>
- 38 J. Hwang, Y. Seo, Y. Jo, J. Son, and J. Choi: *Sci. Rep.* **6** (2016) 34778. <https://doi.org/10.1038/srep34778>
- 39 A. Y. Fadeev, and T. J. McCarthy: *Langmuir* **16** (2000) 7268. <https://doi.org/10.1021/la000471z>
- 40 O. Seitz, P. G. Fernandes, R. Tian, N. Karnik, H. C. Wen, H. Stiegler, R. A. Chapman, E. M. Vogel, and Y. J. Chabal: *J. Mater. Chem.* **21** (2011) 4384. <https://doi.org/10.1039/c1jm10132c>
- 41 R. K. Gupta, A. Periyakaruppan, M. Meyyappan, and J. E. Koehne: *Biosens. Bioelectron.* **59** (2014) 112. <https://doi.org/10.1016/j.bios.2014.03.027>
- 42 L. Guo, Z. Yang, S. Zhi, Z. Feng, C. Lei, and Y. Zhou: *PLoS One* **13** (2018) e0194631. <https://doi.org/10.1371/journal.pone.0194631>
- 43 C. Schmidt, A. Kammel, J. A. Tanner, A. B. Kinghorn, M. M. Khan, W. Lehmann, M. Menger, U. Schedler, P. Schierack, and S. Rödiger: *Sci. Rep.* **12** (2022) 2961. <https://doi.org/10.1038/s41598-022-06817-0>
- 44 T. Hianik, V. Ostatná, M. Sonlajtnerova, and Igor Grman: *Bioelectrochemistry* **70** (2007) 127. <https://doi.org/10.1016/j.bioelechem.2006.03.012>